



This is a repository copy of *Ultrasonic spray deposition of a passivating agent for spray-coated, methylammonium-free perovskite solar cells*.

White Rose Research Online URL for this paper:

<https://eprints.whiterose.ac.uk/206150/>

Version: Published Version

Article:

Cassella, E.J. orcid.org/0000-0003-4897-1650, Thornber, T. orcid.org/0000-0001-7008-3081, Oliver, R.D.J. orcid.org/0000-0003-4980-7940 et al. (7 more authors) (2024)

Ultrasonic spray deposition of a passivating agent for spray-coated, methylammonium-free perovskite solar cells. *Solar RRL*, 8 (2). 2300814. ISSN 2367-198X

<https://doi.org/10.1002/solr.202300814>

Reuse

This article is distributed under the terms of the Creative Commons Attribution (CC BY) licence. This licence allows you to distribute, remix, tweak, and build upon the work, even commercially, as long as you credit the authors for the original work. More information and the full terms of the licence here:

<https://creativecommons.org/licenses/>

Takedown

If you consider content in White Rose Research Online to be in breach of UK law, please notify us by emailing eprints@whiterose.ac.uk including the URL of the record and the reason for the withdrawal request.



eprints@whiterose.ac.uk
<https://eprints.whiterose.ac.uk/>

Ultrasonic Spray Deposition of a Passivating Agent for Spray-Coated, Methylammonium-Free Perovskite Solar Cells

Elena J. Cassella, Timothy Thornber, Robert D. J. Oliver, Mary E. O’Kane, Emma L. K. Spooner, Rachel C. Kilbride, Thomas E. Catley, Onkar S. Game, Alexandra J. Ramadan,* and David G. Lidzey*


Defect management in perovskite solar cells (PSCs) via surface passivation has become a cornerstone in maximizing both stability and solar-to-electrical power conversion efficiency (PCE) of devices by reducing defect densities and/or improving energetic alignment between the perovskite and charge-transporting layers. Despite this, few reports explore the use of roll-to-roll compatible technologies to deposit such interfacial treatments, limiting the applicability of passivation in real-world contexts. In this work, iso-butylammonium bromide (i-BABr) is spray-coated onto a $\text{Cs}_{0.15}\text{FA}_{0.85}\text{PbI}_{2.85}\text{Cl}_{0.15}$ perovskite surface which is deposited using gas-assisted ultrasonic spray coating. It is found that i-BABr treatments result in the formation of a quasi-2D perovskite layer. The spray-coated surface treatment results in an impressive 80 mV improvement in the median open-circuit voltage with respect to untreated devices. Importantly, the spray-coated passivation results in very similar positive benefits to the application of spin-coated treatments demonstrating the promise of the spray-passivation methodology. It is shown that devices created in this manner demonstrate PCEs of up to 21.0% (19.4% stabilized), representing the highest reported efficiency for one-step, spray-coated methylammonium-free PSCs. This work represents the first demonstration of a spray-coated surface passivation treatment that is compatible with high-throughput, roll-to-roll processing.

1. Introduction

Organic–inorganic metal halide perovskite solar cells (PSCs) have become the focus of much research attention due to unprecedented developments in power conversion efficiencies (PCE), increasing from 3.8% up to 26.1% in little over a decade.^[1] To drive this technology toward commercialization, perovskite photovoltaic must simultaneously meet requirements for high efficiency, stability, and low production costs.^[2] While leveled cost of energy requirements are relatively insensitive to the absorber material—provided that lifetime and efficiency requirements are met—the capital expenditure (capex) for module production must be sufficiently low to enable sustainable growth of manufacturing output capabilities. In this regard, solution-processable technologies, such as perovskites, that are capable of extremely high-throughput roll-to-roll manufacturing can lower the capex of upscaling module production by orders of magnitude compared to existing silicon and cadmium telluride technologies.^[3]

E. J. Cassella, T. Thornber, R. D. J. Oliver, M. E. O’Kane, A. J. Ramadan, D. G. Lidzey
Department of Physics and Astronomy
University of Sheffield
Hicks Building, Hounsfield Road, Sheffield S3 7RH, UK
E-mail: a.ramadan@sheffield.ac.uk; d.g.lidzey@sheffield.ac.uk

E. L. K. Spooner
Department of Electrical and Electronic Engineering
Photon Science Institute
University of Manchester
Oxford Road, Manchester M13 9PY, UK

 The ORCID identification number(s) for the author(s) of this article can be found under <https://doi.org/10.1002/solr.202300814>.

© 2023 The Authors. Solar RRL published by Wiley-VCH GmbH. This is an open access article under the terms of the Creative Commons Attribution License, which permits use, distribution and reproduction in any medium, provided the original work is properly cited.

DOI: 10.1002/solr.202300814

R. C. Kilbride
Department of Chemistry
University of Sheffield
Dainton Building, Brook Hill, Sheffield S3 7HF, UK

T. E. Catley
Department of Materials Science and Engineering
University of Sheffield
Sir Robert Hadfield Building, Mappin Street, Sheffield S1 3JD, UK

O. S. Game
Department of Physics
Indian Institute of Technology (IIT)
Indore, Khandwa Road, Simrol, Indore 453552, Madhya Pradesh, India

Spray coating has been demonstrated to fabricate devices at throughput speeds of up to 12 m min^{-1} ; a rate that currently outpaces other roll-to-roll deposition techniques.^[4] As such, spray coating is particularly promising for the cost-effective, sustainable production of PSCs. Furthermore, spray coating is a noncontact deposition method, enabling devices to be fabricated over nonplanar surfaces.^[5] To form a thin film via spray deposition, the precursor solution typically undergoes four stages. Initially, a droplet mist is formed from the precursor solution by forcing the solution through a narrow aperture, or with more sophisticated techniques such as electrospray (where an applied voltage results in electrostatically separated droplets) or ultrasonic atomization (where a piezoelectric transducer vibrates to disperse the solution). The ultrasonic coating is expected to produce a droplet mist with a highly uniform droplet diameter, according to Lang's equation.^[6] Next, the droplet mist is guided to the substrate using a "shaping gas" where the droplets at the surface will coalesce to form a continuous, wet film. Finally, evaporation of the casting solvent triggers film crystallization. Techniques to control the nucleation within the as-cast film are essential for the formation of high-quality perovskite films: vacuum-flash-assisted solution processing,^[7] antisolvent bathing,^[8] plasma treatments,^[9] and gas-assisted solution processing (GASP)^[10] have all been employed to regulate the crystallization dynamics of spray-coated perovskite thin-films.

Despite the industrial relevance of spray coating, there are few demonstrations of spray-coated, hybrid organic–inorganic PSCs that avoid the use of thermally unstable (commercially unfavorable) methylammonium (MA) ions in their formulation.^[11,12] Xia et al. prepared $\text{FA}_{0.9}\text{Cs}_{0.1}\text{PbI}_3$ films by a two-step spin coating/spray-coating method by spray depositing FAI (where FA is formamidinium) onto a spin-coated CsI/PbI_2 film, demonstrating device efficiencies of up to 14.8%.^[13] Yu et al. used a two-step evaporation/spray-coating process to fabricate $\text{Cs}_x\text{FA}_{1-x}\text{PbI}_y\text{Br}_{3-y}$ films which were used to create devices and minimodules with PCEs of 18.21% (0.16 cm^2) and 14.7% (10 cm^2), respectively.^[14] Later, Yu et al. exchanged the solvent used to spray deposit the FAI/Br solution to control the "coffee ring" effect and enhance device performances with a $\text{Cs}_{0.19}\text{FA}_{0.81}\text{PbI}_{2.5}\text{Br}_{0.5}$ absorber layer to 19.17% for small-area devices.^[15] Rolston et al. deposited $\text{Cs}_{0.17}\text{FA}_{0.83}\text{PbI}_3$ films using a one-step, plasma-assisted spray coating technique to create both p-i-n PSCs and minimodules (5.9 cm^2 active area) having efficiencies of up to 18% and 15.2%, respectively.^[4]

MA-free perovskite compositions are typically limited in device efficiency (<25% PCE) with respect to MA-containing devices. A key contributing factor to this performance deficit arises from the difference in solubility between formamidinium (FA) and Cs in solution. The lower solubility of Cs leads to difficulties in controlling the crystallization process to yield uniform perovskite thin films.^[16] The best-performing devices typically require defect management strategies to reduce energetic losses in CsFA-based perovskite compositions.^[17–19] Defect management has been a cornerstone in the improvement of state-of-the-art PSCs in recent years. A large number of approaches have recently been explored, including direct passivation with organic amines, Lewis acids and bases, zwitterionic molecules, polymers, and dimensional engineering of the perovskite surface.^[20,21]

To commercialize PSCs, it is critical to develop interface-passivation strategies that use roll-to-roll compatible technologies. Despite this, few articles report the deposition of surface passivating strategies via such techniques. Notably, Subbiah et al. reported slot-die-coated cysteine hydrochloride to minimize open-circuit voltage losses in MAPbI_3 PSCs.^[22] Recently, Teixeira et al. blade-coated *n*-octylammonium iodide onto a $(\text{FAPbI}_3)_{0.85}(\text{MAPbBr}_3)_{0.15}$ perovskite to form a 2-dimensional (2D) perovskite passivation layer at the surface.^[23] We note, however, that of the various roll-to-roll compatible interface-passivation techniques described above, none report the use of ultrasonic spray coating.

In this work, we develop for the first time, a novel spray-coating process to passivate the top surface of the perovskite film using iso-butylammonium bromide (i-BABr). Note, we focus on the development of ultrasonic spray coating as a proof of concept for the deposition of interface passivation. Specifically, we fabricate a 1.58 eV bandgap $\text{Cs}_{0.15}\text{FA}_{0.85}\text{PbI}_{2.85}\text{Cl}_{0.15}$ active layer using one-step, GASP. We investigate the structural, morphological, and photophysical changes induced by the application of a spray-deposited i-BABr treatment. We show that the alkylammonium cation is found to form a 2D perovskite phase at the film surface, passivating the interface between the perovskite and the hole-transporting layer (HTL). Using this approach, we improve the stabilized PCE of spray-coated devices by up to 2% absolute, arising predominantly from increased photovoltage. To the best of our knowledge, the spray-passivation technique developed herein results in record PCEs for one-step spray-coated MA-free PSCs. Critically, the spray-coated passivation technique is found to match the benefits achieved using a comparable spin-coated passivation treatment, demonstrating the promise of spray-coating for high-efficacy passivation treatment. To the authors' best knowledge, this represents the first demonstration of a spray-cast, surface-passivating posttreatment.

2. Results and Discussion

2.1. Characterization of Spray-Passivated Perovskite Thin Films

In this work, we evaluate the effect of spray-coating iso-butylammonium bromide (i-BABr) onto the surface of a spray-coated, MA-free $\text{Cs}_{0.15}\text{FA}_{0.85}\text{PbI}_{2.85}\text{Cl}_{0.15}$ perovskite active layer. Here, the stoichiometry of the perovskite composition refers to the stoichiometry of the precursor solution. We note, however, that the resulting perovskite film may differ from its solution stoichiometry. We henceforth refer to spray-coated perovskite films without any i-BABr treatment as *pristine* films. Here, we apply one-step, GASP using a Sonotek Exactacoat housed within an N_2 -filled glovebox to spray deposit the perovskite active layer whose deposition conditions were optimized according to our previous work.^[10] Here, we evaluated the precursor ink concentration, substrate temperature during deposition, and delay time between the spray deposition of the precursor solution and application of the gas-jet. We find that the *pristine* spray-coated devices are highly comparable to spin-coated reference cells as can be seen in Supplementary Figure 1 and Table S1 (Supporting Information). Perovskite films were annealed at 70°C for 5 min in an N_2 -filled glovebox, then at 150°C for

10 min in ambient conditions ($\approx 40\%$ relative humidity).^[18] Perovskite films were allowed to cool to room temperature prior to further processing. To spray-passivate films, the spray head was moved in a single pass over the perovskite surface, depositing the i-BABr solution (7.5 mM, isopropanol). The as-cast, wet i-BABr film was observed to dry by evaporation over a period of a few seconds. Spray-passivated films were then annealed at 100 °C for 5 min. See the Experimental Section for full details.

We first investigated the influence of the spray-coated surface treatment on the bulk crystal structure of perovskite thin films using grazing-incidence wide-angle X-Ray scattering (GIWAXS) on spray-coated perovskite films with (*spray*) and without (*pristine*) the spray-coated i-BABr surface treatment. For comparison, we include scattering patterns of a spray-coated perovskite film with a spin-coated i-BABr treatment (*spin*). **Figure 1a–c** shows the 2D GIWAXS patterns collected at an incidence angle of 0.3°, with the 1D integrated patterns shown in **Figure 1d**. For all films, the uniform diffraction rings demonstrate a randomly oriented, highly crystalline 3D perovskite phase, as well as the presence of PbI_2 ($Q = 0.9 \text{ \AA}^{-1}$). Both *spray*- and *spin*-passivated perovskite thin films GIWAXS patterns have additional scattering signals in the out-of-plane direction (Q_z direction in reciprocal space) at lower scattering vectors of $Q = 0.32 \text{ \AA}^{-1}$ and 0.64 \AA^{-1} . These scattering signals correspond to (020) and (040) $n = 2$, 2D perovskite planes that are oriented parallel to the substrate surface.^[24]

We observe weaker intensity 2D-perovskite scattering signals in the GIWAXS pattern for the *spin*-passivated sample as compared to the *spray*-passivated sample. This relative reduction in scattering intensity of 2D perovskite phases may arise from the formation of amorphous regions upon treatment with spin-coated i-BABr. In the spin-coating process, the passivation

treatment has minimal “resting time” on top of the perovskite surface before spin coating induces rapid solvent evaporation. In contrast, the spray-coated i-BABr treatment is left to dry naturally which occurs more slowly. Therefore, i-BABr molecules have more time to react with the underlying material and organize into crystalline order in the case of spray coating when compared to spin coating. Notably, we found that the scattering intensity of the 2D perovskite formed on *spin*-passivated samples was highly variable depending on the exact contact time between the solution and the film prior to beginning the spin-coating program as shown in Supplementary Figure 2 (Supporting Information). X-Ray diffraction (XRD) profiles of *spin*-passivated samples show the appearance of 2D perovskite phases after longer surface contact times prior to starting the spin coating program.

Here, we highlight that a reduced concentration of i-BABr solution was necessary for spray-coated surface treatment (7.5 mM) in comparison to spin-coated surface treatment (15 mM). Due to the increased surface contact time of the solution in the case of spray coating, when spray coated at the higher concentration (15 mM), we detect both a stronger scattering signal originating from 2D perovskite surface layers, and a peak at $Q = 0.45 \text{ \AA}^{-1}$ indexed to a (020) $n = 1$ 2D phase (see Supplementary Figure 3 and Supplementary Figure 4, Supporting Information). The higher scattering intensity likely arises from an increased proportion of 2D material within the probed film volume, indicating the formation of a thicker 2D perovskite layer on top of the underlying 3D film. This was found to significantly limit device performance due to the increased series resistance associated with the insulating organic spacer layers between neighboring inorganic layers, and so was not studied further.

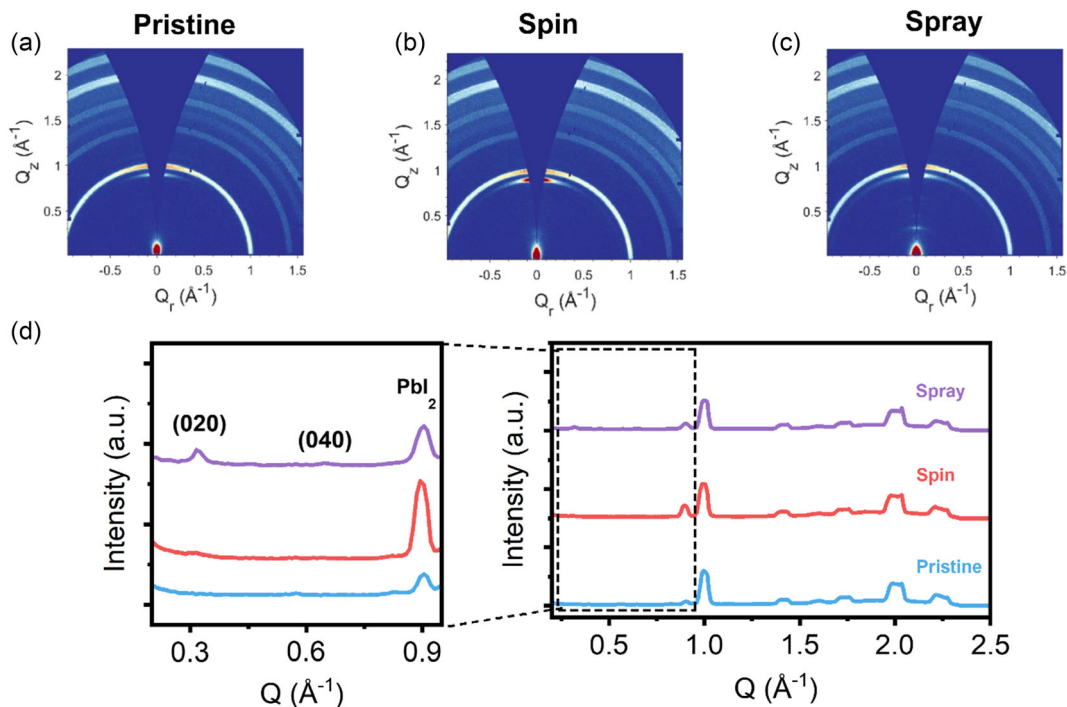


Figure 1. 2D GIWAXS scattering patterns of a) *pristine* (untreated, spray-coated perovskite), b) *spin* (spin-coated i-BABr on spray-coated perovskite), and c) *spray* (spray-coated i-BABr on spray-coated perovskite) films. d) 1D GIWAXS intensity profiles of *pristine* (blue), *spin* (red), and *spray* (purple) films.

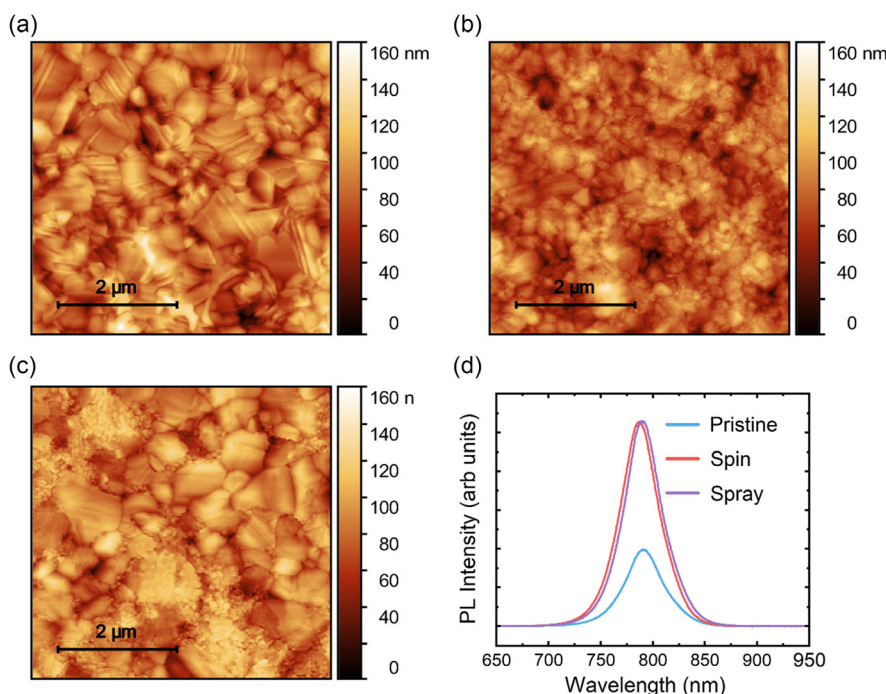


Figure 2. AFM images of a) *pristine*, b) *spin*-passivated, and c) *spray*-passivated perovskite films, with 2 μm scale bar inset. d) Steady-state PL measurements of *pristine*, *spin*, and *spray* films on quartz-coated glass.

Atomic force microscopy (AFM) images indicate a clear difference in the surface topography upon treatment with i-BABr (Figure 2a–c). The untreated *pristine* 3D perovskite surface is characterized by large grains with dimensions up to $\approx 1 \mu\text{m}$. Upon treatment with spin-coated i-BABr, the *spin*-passivated perovskite surface appears to have smaller grain dimensions, coupled with a very slight reduction in the mean value of the root-mean-square roughness (R_{RMS}) from $21.3 \pm 1.5 \text{ nm}$ ($n = 3$ sampled areas, \pm standard error of the mean) to $18.6 \pm 0.5 \text{ nm}$ (see Supplementary Figure 5, Supporting Information). We note that although the standard errors of the mean do not overlap, this is not a definitive indication of statistical significance. However, homogenization of the perovskite surface upon surface treatment follows previous reports,^[25,26] wherein surface passivation reduces the height difference between the grains and grain boundaries. Notably, although regions of reduced domain size are apparent at the surface of *spray*-passivated thin films, the underlying 3D perovskite grain structure remains clearly visible. The mean R_{RMS} of *spray*-passivated films ($21.5 \pm 0.6 \text{ nm}$) remains similar to that of *pristine* films, with significant overlap of the mean R_{RMS} values. Earlier reports have discussed a mechanism by which nonconformal 2D perovskite surface layers provide local passivation, while regions of exposed 3D perovskite enable efficient charge extraction, not limited by the local series resistance of the 2D layers.^[27,28] We suspect that droplet-based roll-to-roll compatible deposition methods such as spray coating and inkjet printing (as opposed to meniscus-based techniques) may be uniquely placed to engineer such discontinuous surface layers over large areas, with such layers capable of combining local passivation with maximal efficacy of charge extraction.

To evaluate the performance of spray-coated i-BABr as a passivating treatment, we measured the steady-state photoluminescence (PL) intensity of the treated and untreated perovskite films (see Figure 2d). Here, we see a clear increase in the PL intensity upon treatment of the spray-coated perovskite with either spin-coated or spray-coated i-BABr. These results indicate that the nonradiative recombination at the perovskite surface has been significantly suppressed upon treatment with i-BABr. Both spin-coated and spray-coated i-BABr treatments improve the PL intensity to a similar level. We also observe a slight blue shift of the λ_{max} of the PL intensities upon surface treatment, from 790 nm for *pristine* films to 787 and 789 nm for *spin*- and *spray*-passivated films, respectively. This wavelength shift might imply incorporation of Br^- into the perovskite lattice.^[29] To investigate this blue shift further, we have recorded XPS data of the *pristine*, *spray*-, and *spin*-passivated films (see Supplementary Figure 6, Supporting Information). Here, as expected, we find that both passivated films demonstrate a clear Br signal which is not observed in the *pristine* film. In these samples, we find that the Br signal is larger in the *spin*-passivated film as compared to the film passivated by spray coating. This finding appears to correlate with the results of the PL measurements where we noted an increased blue shift in the *spin*-passivated sample, suggesting that the origin of the blue shift indeed occurs due to the presence of Br^- introduced by surface passivation.

From the electronic, structural, and morphological characterization techniques, we confirm formation of a 2D layer on top of the 3D perovskite surface for both *spin*- and *spray*-coated i-BABr treatments. By tuning the concentration of the spray-coated i-BABr treatment, we tailor the formation of this 2D layer. To evaluate the efficacy of the passivating treatment, we next investigated the influence of the treatment on photovoltaic device performance.

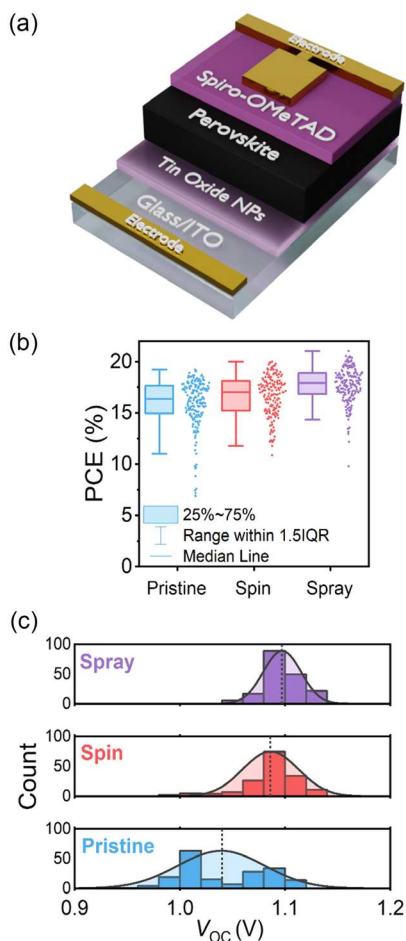


Figure 3. a) Schematic of the *n-i-p* perovskite solar cells with the architecture ITO/SnO₂/Cs_{0.15}FA_{0.85}PbI_{2.85}Cl_{0.15}/Spiro-OMeTAD/Au. b) Boxplot of PCE of *pristine* (untreated spray perovskite, blue, *n* = 93), *spin*-passivated (sprayed perovskite with spin-coated i-BABr treatment, red, *n* = 82), and *spray*-passivated (sprayed perovskite with spray-coated i-BABr treatment, purple, *n* = 92) devices. Histogram plots of c) open-circuit voltage (*V*_{OC}) of *pristine*, *spin*-passivated, and *spray*-passivated devices. Vertical dotted lines indicate the mean value of the normal distribution.

2.2. Photovoltaic Performance of Spray-Passivated Devices

The electron-transporting layer was deposited via a colloidal nanoparticle tin oxide (np-SnO₂) solution which was first spin-coated onto an indium tin oxide cathode under ambient

Table 1. Device performance metrics of cells containing a pristine spray-coated perovskite layer (*pristine*), a spray-coated perovskite layer treated with spin-coated i-BABr (*spin*-passivated), and a spray-coated perovskite layer treated with spray-coated i-BABr (*spray*-passivated). Values are presented as mean ± standard deviation, while champion values are displayed within parentheses. Both forward and reverse *J-V* sweeps are included in the dataset.

Device	<i>J</i> _{SC} [mA cm ⁻²]	<i>V</i> _{OC} [V]	Fill factor [%]	PCE [%]	<i>n</i> _{cells}
<i>Pristine</i>	21.6 ± 1.3 (23.5)	1.04 ± 0.04 (1.11)	70.7 ± 9.7 (79.7)	16.0 ± 2.4 (19.2)	93
<i>Spin</i>	20.3 ± 4.8 (23.5)	1.09 ± 0.03 (1.13)	71.7 ± 12.3 (81.0)	16.7 ± 2.0 (20.0)	82
<i>Spray</i>	21.7 ± 1.2 (24.0)	1.10 ± 0.02 (1.14)	74.0 ± 7.5 (81.0)	17.7 ± 1.8 (21.0)	92

conditions. The Cs_{0.15}FA_{0.85}PbI_{2.85}Cl_{0.15} perovskite active layers and i-BABr treatments were then spray- or spin-coated as described above using an ultrasonic Sonotek Exactacoat system housed within an N₂-filled glovebox. A 2,2',7,7'-Tetrakis[N,N-di(4-methoxyphenyl)amino]-9,9'-spirobifluorene (spiro-OMeTAD) HTL was then spin-coated onto the perovskite films within an N₂-filled glovebox. Full details can be found in the Experimental Section. **Figure 3a** schematically illustrates the architecture of the fabricated *n-i-p* devices.

Figure 3b displays a statistical boxplot of the overall device PCE. Here, the median (champion) PCE of *spray*-passivated devices is improved to 17.9% (21.0%) versus 16.4% (19.2%) for *pristine* cells. **Figure 3c** displays a histogram of the open-circuit voltage (*V*_{OC}) recorded for *pristine*, *spin*-passivated, and *spray*-passivated devices. We find that both spin-coated and spray-coated i-BABr treatments result in a statistically significant increase in the median *V*_{OC} with respect to the *pristine* devices of 70 and 80 mV for *spin*- and *spray*-passivated devices, respectively. This improvement in *V*_{OC} suggests a reduction in nonradiative recombination at the perovskite/HTL interface due to the passivation treatment, a finding in agreement with the PL measurements. Full device performance statistics are tabulated in **Table 1**. The standard deviation from the mean for all device parameters is found to be lower for the *spray*-passivated devices in comparison to both the *pristine* and *spin*-passivated devices. We attribute this to the superior repeatability of the spray-coated passivation treatment, which arises from the programmed control of the spray gantry versus the uncertainty due to the variability associated with spin-coated treatment times.

Figure 4a–d shows the external quantum efficiency (EQE), *J-V* curves, and stabilized outputs of a pair of *pristine* and *spray*-passivated devices. The bandgap of both devices is determined by fitting a sigmoid function to the absorption onset of the EQE spectra.^[30] From the 787 nm inflection point, both *pristine* and *spray*-passivated perovskite films are determined to have a 1.58 eV bandgap. We find the *J*_{SC-EQE} (21.2 and 21.1 mA cm⁻², respectively) to be in good agreement with *J*_{SC-JV} values (22.2 and 22.8 mA cm⁻², respectively) having less than 10% mismatch between the measured current densities.^[31] While we note a 0.6 mA cm⁻² increase in the *J*_{SC-JV} values between these individual devices (a deviation not apparent in the *J*_{SC-EQE} values), we find that across the entire sample set the mean average *J*_{SC-JV} only increases by 0.1 mA cm⁻². In contrast, the mean average *V*_{OC} increases by 60 mV with this value driving the mean average PCE increase of 1.7%. The stabilized power output (SPO) of the best-performing *spray*-passivated device is 19.4%, a value that is 2% absolute higher than the *pristine* device.

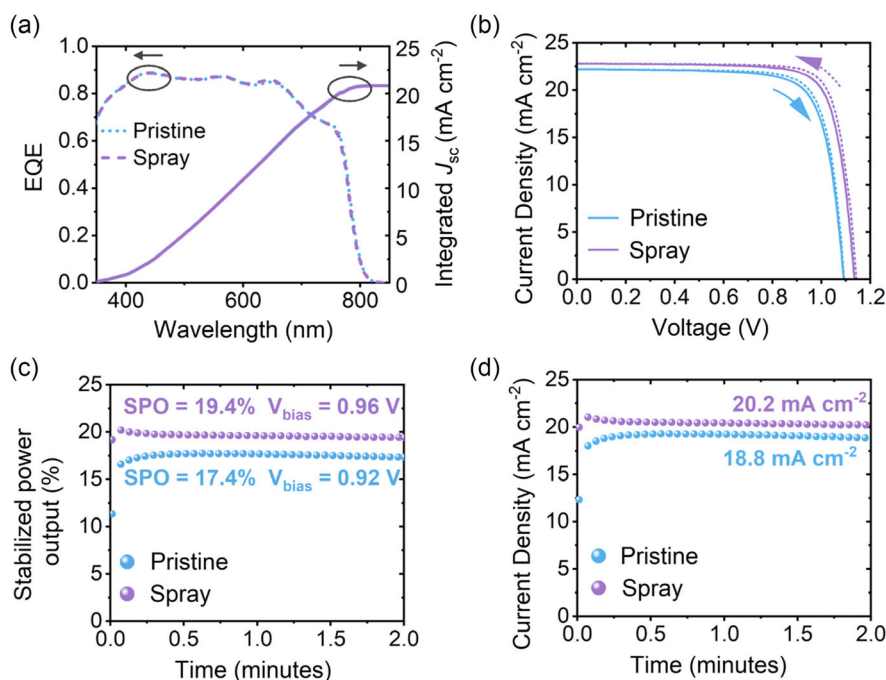


Figure 4. a) EQE, b) J - V curves, c) stabilized PCE, and d) stabilized current density of *pristine* and *spray*-passivated devices.

3. Conclusion

We have demonstrated for the first time the use of a spray-coated, surface-passivating treatment, suitable for high-speed, roll-to-roll processing. By spray depositing iso-butylammonium bromide (i-BABr) onto the surface of spray-coated $\text{Cs}_{0.15}\text{FA}_{0.85}\text{PbI}_{2.85}\text{Cl}_{0.15}$ films, we form a 2D perovskite layer at the thin film surface, as confirmed by GIWAXS measurements. Dimensional engineering of the perovskite surface was found to suppress nonradiative recombination losses at the perovskite/HTL interface. This spray-passivation treatment was found to improve the median V_{OC} of devices by 80 mV with respect to cells based on an untreated, spray-coated perovskite active layer. Importantly, we find the spray-coated passivating treatment to be highly reproducible, reducing the standard deviation from the mean for all device performance metrics in comparison to a spin-coated surface treatment. Using this approach, we demonstrate the highest reported performance for one-step spray-coated, MA-free PSCs. This result represents proof of concept of the deposition of surface passivation treatments, which are key to unlock the performance potential of devices, onto perovskite layers via spray coating in an industrially relevant roll-to-roll compatible manner.

4. Experimental Section

Materials: All materials and solvents were used as received without any further purification. PbI_2 (99.99% trace metals basis) was purchased from TCI Chemicals. 2,2',7,7'-Tetrakis[N,N-di(4-methoxyphenyl)amino]-9,9'-spirobifluorene (spiro-OMeTAD, >99.5% purity), formamidinium iodide (FAI, >99.5% purity), iso-butylammonium bromide (i-BABr, >98%), and prepatterned 20 mm \times 15 mm ITO-coated glass substrates ($\approx 20 \Omega/\square$) were purchased from Ossila. All other solvents and materials, including PbCl_2 (99.999% trace metals basis) and CsI (99.999% trace

metals basis), were purchased from Sigma Aldrich unless otherwise stated. Substrates were rinsed sequentially by sonification in diluted Helmanex solution, boiling deionized water, acetone, and isopropanol (IPA). Following this, substrates were dried under a flow of N_2 and UV ozone treated for at least 15 min prior to further device processing. All perovskite solutions were filtered through a 0.2 μm polytetrafluoroethylene (PTFE) filter.

Device Fabrication: Spin-Coated Layers: To deposit nanoparticle- SnO_2 electron transport layers, a colloidal SnO_2 solution (15 wt% in H_2O , Alfa Aesar) diluted 1:4 in deionized water was statically spin coated at 3000 rpm for 30 s, prior to annealing at 150 $^\circ\text{C}$ for 30 min and then UV ozone treated for a further 20 min. A 2 M $\text{Cs}_{0.15}\text{FA}_{0.75}\text{PbI}_{2.85}\text{Cl}_{0.15}$ precursor ink was prepared according to previously reported procedures.^[18] Briefly, 1 mL of the precursor solution contained 285.5 mg FAI, 922 mg PbI_2 , 55.6 mg of PbCl_2 , and 88.3 mg CsI dissolved in 1 mL of DMF. 192.9 μL of N-methyl-2-pyrrolidone (NMP) was added to the 2 M precursor solution. The precursor solution was spin-coated onto SnO_2 -coated substrates in an N_2 -filled glovebox at 5000 rpm for 50 s, before annealing at 70 $^\circ\text{C}$ for 5 min inside the glovebox and then at 150 $^\circ\text{C}$ for 10 min in a $\approx 40\%$ RH ambient cleanroom. Spin-passivated substrates had 50 μL of a 15 mM solution of i-BABr in IPA statically deposited and subsequently spun at 4000 rpm for 20 s, before being annealed on a hot plate at 100 $^\circ\text{C}$ for 5 min. Spiro-OMeTAD (86 mg mL⁻¹) was dissolved in chlorobenzene, then doped with 34 μL mL⁻¹ 4-tert-butyl-pyridine, 20 μL mL⁻¹ of a lithium bis(trifluoromethanesulfonyl)imide solution (500 mg mL⁻¹ in acetonitrile) and 11 μL of FK209 solution (FK209 Co(III) TFSI salt, 300 mg mL⁻¹ in acetonitrile). The solution was thoroughly vortex mixed and filtered through a 0.2 μm PTFE filter before spin coating dynamically at 4000 rpm for 30 s. The spiro-OMeTAD-coated devices were left to oxidize overnight in a dry box.

Device Fabrication: Spray-Coated Layers: A 1.1 M $\text{Cs}_{0.15}\text{FA}_{0.75}\text{PbI}_{2.85}\text{Cl}_{0.15}$ precursor ink was prepared by dilution from a 2 M precursor ink. The 1.1 M ink was spray-coated in a nitrogen-filled glovebox using a Sonotek Exactacoat system. The substrate was held at 30 $^\circ\text{C}$ in the optimized protocol described in the main text. A motorized gantry moved the spray head over the substrate surface at a speed of 80 mm s⁻¹ and a tip-surface separation of around 10 cm. The precursor ink was delivered at a flow rate of 1 mL min⁻¹ through a tip driven at 2 W and directed to the substrate

surface by an N₂ gas flow at a pressure of 3 psi. After a short delay time (25 s for optimized devices), an air knife (Meech A8 80 mm Air Knife, RS Components) was passed over the substrate surface at a speed of 3 mm s⁻¹ and a distance of around 2 cm, blowing ambient-temperature N₂ at a pressure of 20 psi and an angle of 45° from the surface normal. The perovskite films were subsequently annealed at 70 °C for 5 min in the glovebox, and then at 150 °C in ambient conditions in a ≈40%RH clean-room. Spray passivation was then performed within an N₂-filled glovebox. For spray-passivated films, an i-BABr solution (either 7.5 mM or 15 mM in IPA) was delivered to the spray head at a flow rate of 1.5 mL min⁻¹. A piezoelectric tip operated at 1 W formed a droplet mist which was directed at the substrate by a flow of N₂ at a pressure of 3 psi. In our optimized process, the spray head passed once over the substrate held at room temperature at a speed of 40 mm s⁻¹. The spray-passivated films were allowed to evaporate and then annealed at 100 °C for 5 min.

Device Fabrication: Evaporated Layers and Contacts: Device layers were patterned using a razorblade before evaporation of an Au (Cooksongold, 80 nm) back contact through a shadow mask at 0.1–1.0 Å s⁻¹.

Device Characterization: Current–Voltage Measurements: *J–V* measurements were recorded using a Newport 92251A-1000 solar simulator in ambient conditions without any preconditioning of cells. The simulated Air Mass (AM) 1.5 spectrum was calibrated to 100 mW cm⁻² at the substrate holder location using an NREL-certified silicon reference cell. Metal aperture masks with accurately determined areas of 0.023 cm² were used to define the measurement active area. Devices were swept between –0.1 and 1.2 V at 50 mV s⁻¹ using a Keithley 237 source-measure unit. The devices were held at V_{MPP} for SPO measurements.

Device Characterization: EQE: EQE measurements were recorded over a wavelength range of 325–900 nm using a QuantX-300 Quantum Efficiency Measurement System. The system was equipped with a 100 W Xenon arc lamp chopped at 25 Hz and focused through an Oriel Monochromator (CS130B).

Device Characterization: XRD: A PANalytical X'Pert Pro system equipped with a Copper Line Focus X-Ray tube run at 45 kV with a tube current of 40 mA recorded XRD patterns at room temperature. The diffractometer operated in Bragg–Brentano geometry to record diffraction patterns from 5.00° to 99.99° 2θ.

Device Characterization: AFM: AFM (Veeco Dimension 3100) images were collected in intermittent contact (tapping) mode with a NuNano Scout 350 cantilever (nominal spring constant 42 N m⁻¹, resonant frequency 350 kHz). Each sample was scanned over three separate 5 × 5 μm areas with a resolution of 512 × 512 pixels.

Device Characterization: GIWAXS: GIWAXS measurements were performed using a Xeuss 2.0 SAXS/WAXS laboratory beamline (Xenocs) equipped with a liquid Ga MetalJet X-Ray source (Excillum) and a Pilatus 1 M pixel detector (Dectris). X-rays were collimated in “high-flux” mode (S₁ = 1.2 mm, S₂ = 1.2 mm, S₃ = 0.8 mm, S₄ = 0.8 mm) and directed onto the sample surface at a grazing incidence angle of 0.3°. The entire flight path was held under vacuum during measurement to reduce background air scatter. The detector was positioned ≈300 mm from the sample. This distance was calibrated using a silver behenate standard in transmission geometry. Data were corrected, reshaped, and reduced using the GIXSGUI MATLAB toolbox.^[32] 1D intensity Q-dependent profiles were extracted by azimuthally integrating the 2D images across the full azimuthal range. Perovskite films for GIWAXS were prepared for devices, being deposited on top of SnO₂-coated ITO substrates.

Device Characterization: Steady-State PL: The samples were excited using a 405 nm CW laser (Edmund Optics 50 mW Turnkey laser) from the sample side at 240 mWcm⁻². PL was collected from the sample side and fiber-coupled into a spectrometer (OceanOptics Flame). Care was taken to ensure that each sample was of approximately the same thickness and that it was in focus to ensure that PL intensities could be compared.

Supporting Information

Supporting Information is available from the Wiley Online Library or from the author.

Acknowledgements

E.J.C. and T.T. contributed equally to this work. This work was funded by the Engineering and Physical Sciences Research Council (EPSRC) grants EP/S009213/1 (The integration of photovoltaic devices with carbon-fiber composites), EP/V027131/1 (High-efficiency flexible and scalable halide-perovskite solar modules), and EP/T012455/1 (Molecular photonic breadboards). E.J.C. and E.L.K.S. thank the EPSRC for a Ph.D. studentship from the Centre for Doctoral Training in New and Sustainable PV, (EP/L01551X/1). T.T. and T.E.C. thank the Faculty of Science, University of Sheffield for a studentship. M.E.O'K. thanks to the EPSRC for a Ph.D. studentship from the Centre for Doctoral Training in Polymers and Colloids, (EP/L016281/1). The authors also acknowledge the EPSRC for the capital equipment grants to purchase (EP/M028437/1) and upgrade (EP/V034804/1) the laboratory-based Xenocs/Excillum X-Ray scattering instrument. The authors acknowledge and thank Akash Dasgupta for assistance with measurements. The authors also acknowledge and thank Dr Debbie Hammond and the Sheffield Surface Analysis Centre for assistance with XPS measurements.

Conflict of Interest

The authors declare no conflict of interest.

Data Availability Statement

The data that support the findings of this study are available from the corresponding author upon reasonable request.

Keywords

perovskites, spray coating, surface passivation

Received: October 24, 2023

Published online:

- [1] NREL, Best Research Cell Efficiencies, can be found under <https://www.nrel.gov/pv/cell-efficiency.html>, **2023**.
- [2] F. Yang, D. Jang, L. Dong, S. Qiu, A. Distler, N. Li, C. J. Brabec, H. Egelhaaf, *Adv. Energy Mater.* **2021**, *11*, 2101973.
- [3] K. Bruening, B. Dou, J. Simonaitis, Y. Y. Lin, M. F. A. M. van Hest, C. J. Tassone, *Joule* **2018**, *2*, 2464.
- [4] N. Rolston, W. J. Scheideler, A. C. Flick, J. P. Chen, H. Elmaraghi, A. Sleugh, O. Zhao, M. Woodhouse, R. H. Dauskardt, *Joule* **2020**, *4*, 2675.
- [5] T. Thornber, O. S. Game, E. J. Cassella, M. E. O'Kane, J. E. Bishop, T. J. Routledge, T. I. Alanazi, M. Togay, P. J. M. Isherwood, L. C. Infante-Ortega, D. B. Hammond, J. M. Walls, D. G. Lidzey, *ACS Appl. Mater. Interfaces* **2022**, *14*, 37587.
- [6] R. J. Lang, *J. Acoust. Soc. Am.* **1962**, *34*, 6.
- [7] J. E. Bishop, J. A. Smith, C. Greenland, V. Kumar, N. Vaenas, O. S. Game, T. J. Routledge, M. Wong-Stringer, C. Rodenburg, D. G. Lidzey, *ACS Appl. Mater. Interfaces* **2018**, *10*, 39428.
- [8] S. Uličná, B. Dou, D. H. Kim, K. Zhu, J. M. Walls, J. W. Bowers, M. F. A. M. van Hest, *ACS Appl. Energy Mater.* **2018**, *1*, 1853.
- [9] F. Hilt, M. Q. Hovish, N. Rolston, K. Brüning, C. J. Tassone, R. H. Dauskardt, *Energy Environ. Sci.* **2018**, *11*, 2102.
- [10] E. J. Cassella, E. L. K. Spooner, T. Thornber, M. E. O'Kane, T. E. Catley, J. E. Bishop, J. A. Smith, O. S. Game, D. G. Lidzey, *Adv. Sci.* **2022**, *9*, 2104848.
- [11] S.-H. Turren-Cruz, A. Hagfeldt, M. Saliba, *Science* **2018**, *362*, 449.

- [12] J. E. Bishop, J. A. Smith, D. G. Lidzey, *ACS Appl. Mater. Interfaces* **2020**, *12*, 48237.
- [13] X. Xia, W. Wu, H. Li, B. Zheng, Y. Xue, J. Xu, D. Zhang, C. Gao, X. Liu, *RSC Adv.* **2016**, *6*, 14792.
- [14] X. Yu, X. Yan, J. Xiao, Z. Ku, J. Zhong, W. Li, F. Huang, Y. Peng, Y. B. Cheng, *J. Chem. Phys.* **2020**, *153*, <https://doi.org/10.1063/5.0012803>.
- [15] X. Yu, J. Li, Y. Mo, T. Xiang, Z. Ku, F. Huang, F. Long, Y. Peng, Y.-B. Cheng, *J. Energy Chem.* **2022**, *67*, 201.
- [16] S. Tang, S. Huang, G. J. Wilson, A. Ho-Baillie, *Trends Chem.* **2020**, *2*, 638.
- [17] W. Chen, H. Zhu, S. Wu, J. Yao, R. Chen, M. Pan, W. Chen, J. Zhou, W. Zhang, T. Wang, *J. Mater. Chem. A* **2019**, *7*, 21476.
- [18] T. Bu, J. Li, H. Li, C. Tian, J. Su, G. Tong, L. K. Ono, C. Wang, Z. Lin, N. Chai, X.-L. Zhang, J. Chang, J. Lu, J. Zhong, W. Huang, Y. Qi, Y.-B. Cheng, F. Huang, *Science* **2021**, *372*, 1327.
- [19] Z. Li, M. Wu, L. Yang, K. Guo, Y. Duan, Y. Li, K. He, Y. Xing, Z. Zhang, H. Zhou, D. Xu, J. Wang, H. Zou, D. Li, Z. Liu, *Adv. Funct. Mater.* **2023**, *33*, 2212606.
- [20] G. Wu, R. Liang, M. Ge, G. Sun, Y. Zhang, G. Xing, *Adv. Mater.* **2022**, *34*, 2105635.
- [21] H. Zhang, L. Pfeifer, S. M. Zakeeruddin, J. Chu, M. Grätzel, *Nat. Rev. Chem.* **2023**, *7*, 632.
- [22] A. S. Subbiah, F. H. Isikgor, C. T. Howells, M. De Bastiani, J. Liu, E. Aydin, F. Furlan, T. G. Allen, F. Xu, S. Zhumagali, S. Hoogland, E. H. Sargent, I. McCulloch, S. De Wolf, *ACS Energy Lett.* **2020**, *5*, 3034.
- [23] C. Teixeira, R. Fuentes-Pineda, L. Andrade, A. Mendes, D. Forgács, *Mater. Adv.* **2023**, *4*, 3863.
- [24] Y. Liu, S. Akin, A. Hinderhofer, F. T. Eickemeyer, H. Zhu, J. Seo, J. Zhang, F. Schreiber, H. Zhang, S. M. Zakeeruddin, A. Hagfeldt, M. I. Dar, M. Grätzel, *Angew. Chem.* **2020**, *132*, 15818.
- [25] Q. Jiang, Y. Zhao, X. Zhang, X. Yang, Y. Chen, Z. Chu, Q. Ye, X. Li, Z. Yin, J. You, *Nat. Photonics* **2019**, *13*, 460.
- [26] M. G. La-Placa, L. Gil-Escrig, D. Guo, F. Palazon, T. J. Savenije, M. Sessolo, H. J. Bolink, *ACS Energy Lett.* **2019**, *4*, 2893.
- [27] M. A. Mahmud, H. T. Pham, T. Duong, Y. Yin, J. Peng, Y. Wu, W. Liang, L. Li, A. Kumar, H. Shen, D. Walter, H. T. Nguyen, N. Mozaffari, G. D. Tabi, G. Andersson, K. R. Catchpole, K. J. Weber, T. P. White, *Adv. Funct. Mater.* **2021**, *31*, 2104251.
- [28] W. Peng, K. Mao, F. Cai, H. Meng, Z. Zhu, T. Li, S. Yuan, Z. Xu, X. Feng, J. Xu, M. D. McGehee, J. Xu, *Science* **2023**, *379*, 683.
- [29] T. Jesper Jacobsson, J.-P. Correa-Baena, M. Pazoki, M. Saliba, K. Schenk, M. Grätzel, A. Hagfeldt, *Energy Environ. Sci.* **2016**, *9*, 1706.
- [30] O. Almora, C. I. Cabrera, J. Garcia-Cerrillo, T. Kirchartz, U. Rau, C. J. Brabec, *Adv. Energy Mater.* **2021**, *11*, 2100022.
- [31] M. Saliba, L. Etgar, *ACS Energy Lett.* **2020**, *5*, 2886.
- [32] Z. Jiang, *J. Appl. Crystallogr.* **2015**, *48*, 917.